NRIAG JOURNAL OF ASTRONOMY AND GEOPHYSICS
2020, VOL. 9, NO. 1, 572–585
https://doi.org/10.1080/20909977.2020.1818532

Geodynamics of the Egyptian side of eastern Mediterranean region: preliminary results

Abdel-Monem S. Mohamed[a], Nadia AbouAly[a], Esraa E. Hegazy[a], Matthias Becker[b] and Mohamed Saleh[a]

[a]Geodynamic Department, National Research Institute of Astronomy and Geophysics, Helwan, Egypt; [b]Institute of Physical and Satellite Geodesy, Technical University, Darmstadt, Germany

ABSTRACT

Eastern Mediterranean has been identified as an ideal natural laboratory for studying the kinematics and dynamics of plate interactions because of the wide variety of tectonic processes encompassed, including various stages of continental collision, subduction of oceanic lithosphere and associated back-arc spreading and continental extension. The tectonic framework of the eastern Mediterranean is dominated by the collision of the Arabian and Nubian plates with Eurasia. The interaction of Nubian, Arabian, Eurasian plates and Sinai sub-plate, is the main factor for the seismicity and crustal deformation of Egypt. For the purpose of studying the crustal deformation of Egypt, a set of thirteen GPS stations that covers the time span 2013–2014 is used. For the sake of datum definition and to set a good configuration around the Egyptian stations, we processed 123 international permanent stations with the Egyptian sites using Bernese V.5.2. The estimated absolute horizontal velocity of the Egyptian stations including Nubian plate motion is about 28–30 ± 0.7 mm/yr towards the northeast direction. In Nubia fixed frame, most of the Egyptian sites show insignificant velocity rates, while with respect to Eurasia, we estimated a velocity rate of 6.7 ± 0.6 mm/yr towards the north to northwest direction. Even with only two years of GPS data, our solution is comparable to the previously published rates.

ARTICLE HISTORY
Received 25 June 2019
Revised 23 August 2020
Accepted 28 August 2020

KEYWORDS
Eastern Mediterranean region; Egypt; GNSS data and Seismic data

1. Introduction

The region of Eastern Mediterranean is considered as one of the ideal areas for monitoring kinematics and dynamics interactions between plates (Plag 1998). It encompassed variety of tectonic processes either on large-scale (continental collision, oceanic lithosphere subduction and continental extension) or small-scale processes which have been associated with Nubian, Arabian and Eurasian plate interaction. The collision between these plates affected the tectonic framework of this region which is considered as one of the most attracted areas from both seismic and tectonic visions. The activities at the plate boundaries affect nearly all the countries in the area including Egypt.

Many Authors attempted to constrain crustal movement in Egypt and interaction of Nubian plate with the surrounding tectonic plates (e.g. (McClusky et al. 2000); (McClusky et al. 2003); (Reilinger et al. 2006)), as shown in Figure 1. They provided the rapid motion describing Arabian Peninsula, parts of Iran and Anatolia/Aegean region of about 20–30 mm/yr. Although, these studies had suffered from the deficiency of GPS stations which cover Egypt. (Saleh and Becker 2014) used more than 60 Egyptian (permanent and campaign) stations covering the period 2006–2012. Based on their results, the area showed an average ITRF2008 horizontal velocity of about 30 ± 1.1 mm/yr towards northeast direction. In this study we attempt to introduce horizontal velocity field of northeastern corner of Africa using GPS data of 130 stations (13 stations are permanent and belonging to the Egyptian Permanent GPS Network (EPGN) covering the period from 2013 to 2014).

In 1984 and after the 14 November 1981 earthquake at Kalabsha, southwest of Aswan, a program for monitoring the recent crustal movements and its relation to seismic activity has been established by the National Research Institute of Astronomy and Geophysics (NRIAG). At the beginning of this program, terrestrial methods were applied around the active faults to northwest of lake Nasser. Later, the Global Positing System (GPS) was applied. It was utilised around the seismic active areas in Egypt such as the Nile Valley, Abu-Dabbab, Greater Cairo and Gulf of Suez. In 2006, NRIAG started the

CONTACT Abdel-Monem S. Mohamed abdel_monem@yahoo.com Crustal Movements Laboratory, Geodynamics Department, National Research Institute of Astronomy and Geophysics

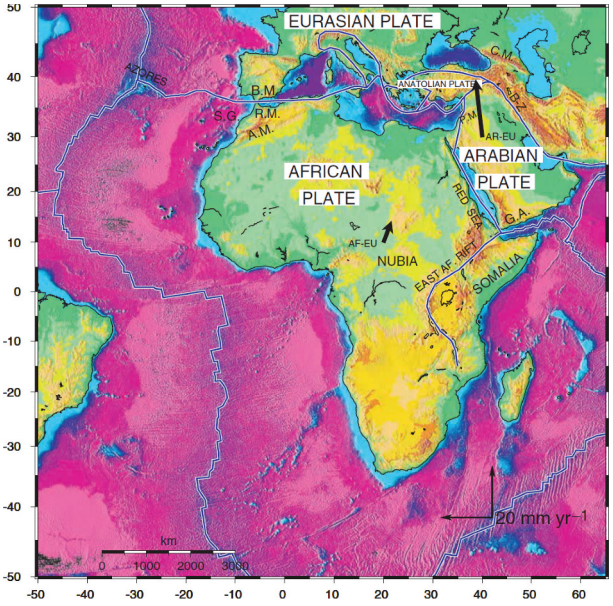

Figure 1. Plate motion map of Arabia-Nubia-Eurasia zone (After (McClusky et al. 2003)).

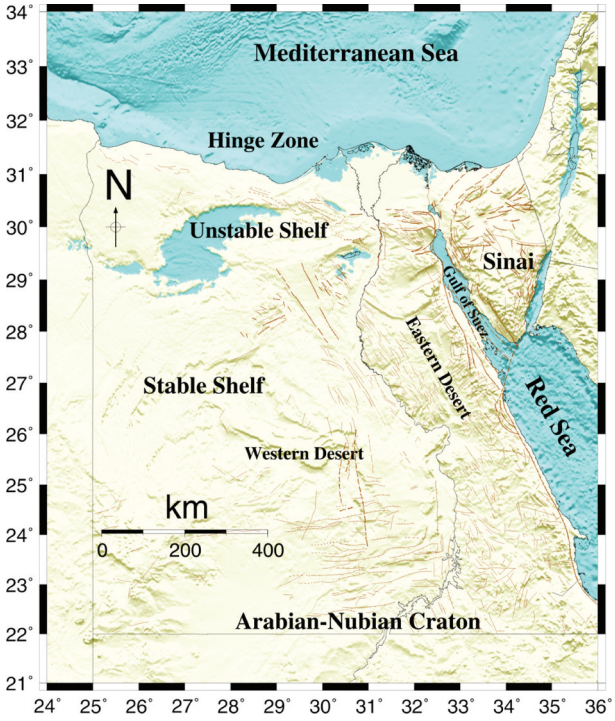

Figure 2. Major geological provinces in Egypt (after (Meshref 1999)).

establishment of the Egyptian Permanent GPS Network (EPGN). This network started only with four stations and gradually this number is still being increased to cover most of the Egyptian territory.

2. Tectonic setting of Egypt

According to many authors (e.g: (Neev 1977); (Orwig 1982); (Harms and Wray 1990); (Zeyen et al. 1997); (Abd El-Motaal and Kusky 2003), (Mosconi et al. 1996); (Stanley and Goodfriend 1997) and (Meshref 1999)), different tectonic features affected Egypt, the structural patterns and tectonics of northeastern corner of the Nubian plate, southeast of Mediterranean Sea and tectonic setting of Sinai sub-plate and Rift System of the Gulf of Suez-Red Sea. The tectonic features have been characterised by three major boundaries of tectonic plates (Plate margin of Red Sea and Nubia-Eurasia and Levant Transform Fault). These boundaries separate the three plates (Nubia, Eurasia and Arabia). After (Said 1962), Egypt is divided into four major geological provinces; the Arabian-Nubian Shield, the stable and unstable shelf, hinge zone and miogeosyncline (Figure 2).

3. Seismicity of Egypt

Although, Egypt is not considered as a major seismic zone, the earthquakes indicate a significant threat. Almost all activities were accompanied with tectonic features along the borders of the three tectonic plate boundaries (Arabia, Nubia and Eurasia). Many authors have carried out detailed studies on the seismicity of Egypt (e.g. (Sieberg 1932); (Gergawi and El Khashab 1968); (Kebeasy 1990); (Abou Elenean 1997); (Abou Elenean 2007); (Badawy 2005) and (Hussein et al. 2006)). Due to the relative motions along the tectonic plates boundaries, the earthquake activities are small to moderate and the highest rates of seismicity are recorded at the eastern boundaries of Egypt and northern part of the Red Sea.

In Egypt, epicentres of earthquake are distributed along three major trends. These trends are extended along the Gulf of Suez through Cairo and Suez, the NE (East Mediterranean) to the SW (Cairo-El-Faiyum) and the Levant – Aqaba trend which has been related to the active sinistral movement along the Levant fault system and the Gulf of Aqaba (Said 1990).

Before 1980, the northeastern corner of Africa suffered from the deficiency of seismic stations, so the activity is scattered. After the 14 November 1981 earthquake (M_L = 5.5) southwest of the High Dam, NRIAG started to install a digital telemetry Network (ALN) around the northern part of lake Nasser. On 12 October 1992, another earthquake with a magnitude of 5.9 happened at Dahshour area, 35 km southwest of Cairo city. It produced a widespread loss in different cities. Therefore, NRIAG installed the Egyptian National Seismic Network (ENSN) which leads to record more seismic events with high accuracy, as shown in Figure 3. (Abou Elenean 2007) has shown that Egypt has suffered from events of interplate and intraplate depending on spatial spreading of modern earthquake foci.

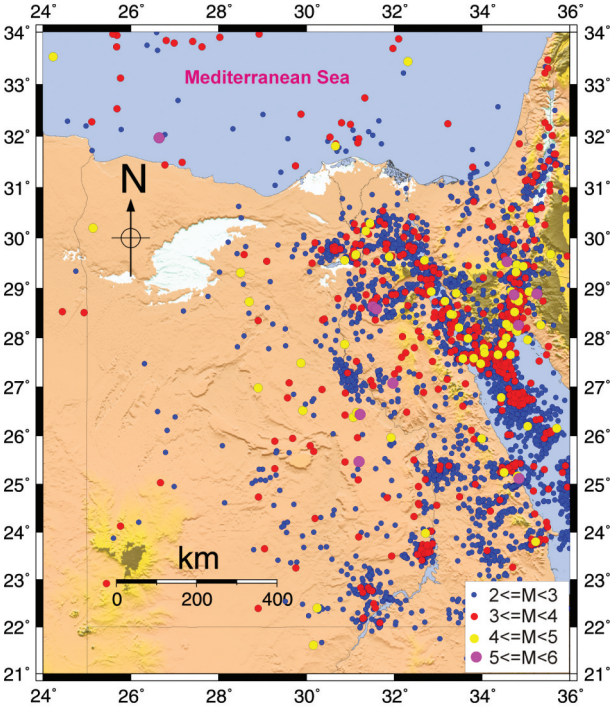

Figure 3. Seismic activity of Egypt recorded by ENSN for the period 1997 to 2014

Figure 3. Seismic activity of Egypt recorded by ENSN for the period 1997–2014.

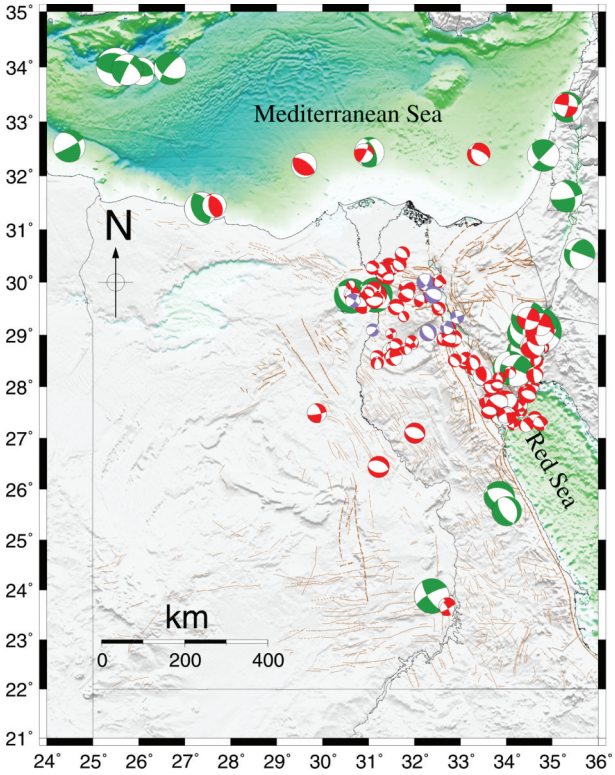

Figure 4. Focal mechanisms for earthquakes occurred in Egypt for the period 1976–2014. Greens are CMT solution from CMT http://www.globalcmt.org/CMTsearch.html and Reds are the solution from ((Mohamed et al. 2016); (Abudeif and Attia 2014); (Sawires et al. 2014); (Badawy et al. 2015); (Badawy et al. 2008); (Abd El-AaL 2010); (Abou Elenean 2007)).

The Focal mechanism solution for some earthquakes happened in Egypt through the period 1976–2014 were collected from different sources as shown in Figure 4.

4. Data processing

In this study we used 13 stations from Egyptian Permanent GPS Network (EPGN), which cover most of Egyptian territory. Three of these stations were used here for the first time, these stations are SAID and MTRH at the Mediterranean coastline and ASWN north of lake Nasser. The GPS data covered the period from 2013 to 2014. Figure 5 shows the geographic distribution of Egyptian Permanent GPS stations. The collected GPS data used in this study is shown in Figure 6, while Table 1 shows the equipment used at these sites.

4.1. Processing steps

Beside the data from EPGN, we downloaded data from 123 international stations from different sources: International GNSS Service (IGS), University NAVSTAR Consortium (UNAVCO), Scripps Orbit and Permanent Array Centre (SOPAC) and EUREF Permanent Network (EPN) starting from the first of 2013 to the end of 2014. These stations were selected to surround Egyptian sites from all direction North, East and South except from West due to the lack of stations, as presented in Figure 7. These stations are belonging to African plate including (Nubian, Somalian, Lwandle and Sinai sub-plate), Arabian and Eurasian plate. Thirty-one out of these 123 stations are included in the International Terrestrial Reference Frame 2008 (ITRF2008) (Altamimi et al. 2011) and were used for datum definition. Bernese software V.5.2 (Dach et al. 2007) was used to process data using the following computational approach:

1- ITRF2008 Reference frame.

2- Final orbits, satellite clocks and final Earth orientation parameters of IGS.

3- Usage of OBS-MAX strategy to form automatic baselines.

4- Usage of quasi-ionosphere-free (QIF) strategy for phase ambiguity resolution.

5- Ionosphere-free frequency L3

6- Elevation cut-off angle 3°

7- Usage of Dry Niell with Global mapping function (GMF) Tropospheric model.

A set of 730 daily normal equations were generated. These normal equations were combined together using ADDNEQ2 (The combination tool in Bernese

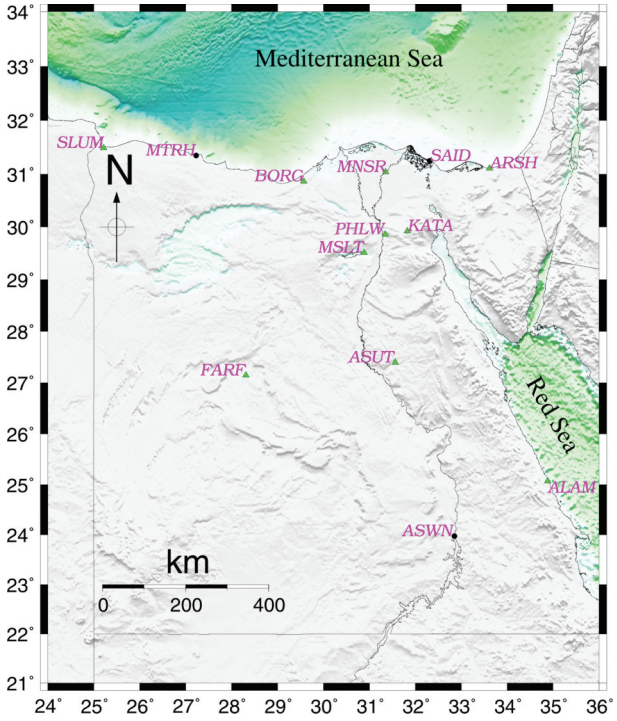

Figure 5. Geographic distribution of Egyptian permanent GPS network (EPGN) stations represented as green triangles while black dots are the unpublished new stations.

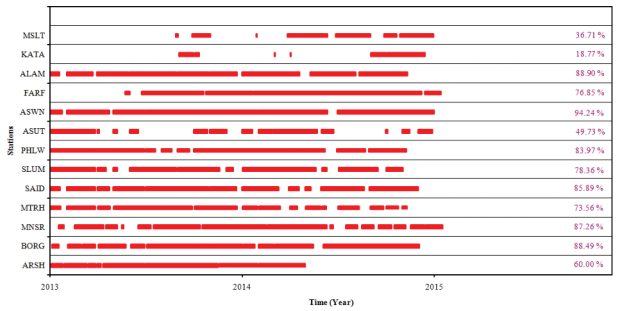

Figure 6. Chart availability of EPGN stations.

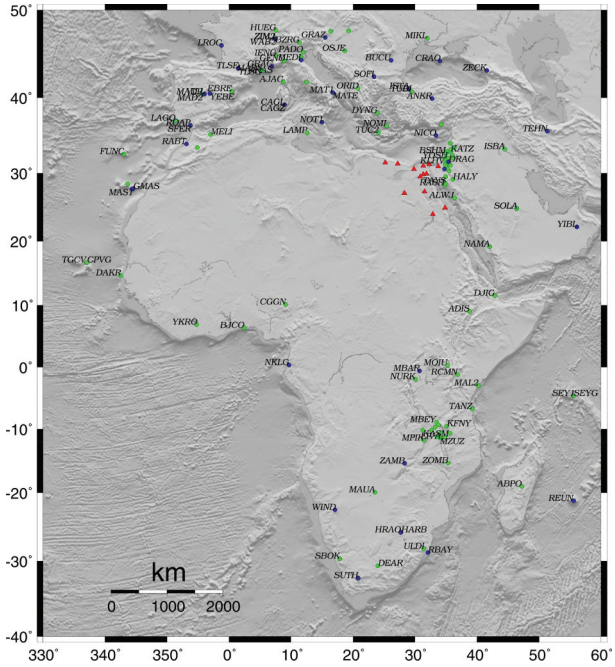

Figure 7. Permanent Egyptian stations are the red triangles and the international stations (IGS, EPN, UNAVCO and SOPAC) are the green circles. Stations used for the datum definition are marked as blue circles.

software) and applying minimum constrained solution to ITRF2008 datum definition which represented by 31 IGS stations. Station position, velocity, standard deviation and residuals for all stations and also variance-covariance matrix were obtained as a result of the combination process. To check the quality of obtained results we made a comparison between the coordinates obtained from the combined solution and the ITRF2008 coordinates using Helmert Transformation as shown in Table A1 in the appendix.

The obtained standard deviations of velocities and coordinates from the daily solution is unrealistic and too optimistic due to the absence of suitable models for time correlation in the GNSS data. Therefore, we used the repeatability to compute more realistic standard deviations. The repeatability of both EPGN and international stations are shown in Figure 8a and b, respectively. For EPGN and international stations, the repeatability ranges from 1 to 4 mm for the horizontal component and 6 to 11 mm for the vertical component. Scaled error can be calculated using the repeatability values for each component as well as the Bernese formal error.

Table 1. Equipment used at Egyptian permanent GPS stations.

Station	4-ID character	Antenna	Receiver	Antenna height	Organised by
Al-Arish	ARSH	TRM55971.00	Trimble NETR5	0.0000	NRIAG
Borg el-arab	BORG	TRM55971.00	Trimble NETR5	0.0000	NRIAG
Mansoura	MNSR	TRM55971.00	Trimble NETR5	0.0000	NRIAG
Marsa Matrouh	MTRH	TRM55971.00	Trimble NETR5	0.0000	NRIAG
Port Said	SAID	TRM55971.00	Trimble NETR5	0.0000	NRIAG
Aswan	ASWN	TRM55971.00	Trimble NETR5	0.0000	NRIAG
Marsa Alam	ALAM	TRM55971.00	Trimble NETR5	0.0000	NRIAG
Helwan	PHLW	TRM41249.00	Trimble 5700	0.0000	NRIAG
Saloum	SLUM	TRM41249.00	Trimble 5700	0.0000	NRIAG
Katameya	KATA	TRM41249.00	Trimble 5700	0.0000	NRIAG
Meslat	MSLT	TRM41249.00	Trimble R7	0.0000	NRIAG
Farafra	FARF	TRM41249.00	Trimble 5700	0.0000	NRIAG
Asuit	ASUT	TRM41249.00	Trimble 5700	0.0000	NRIAG

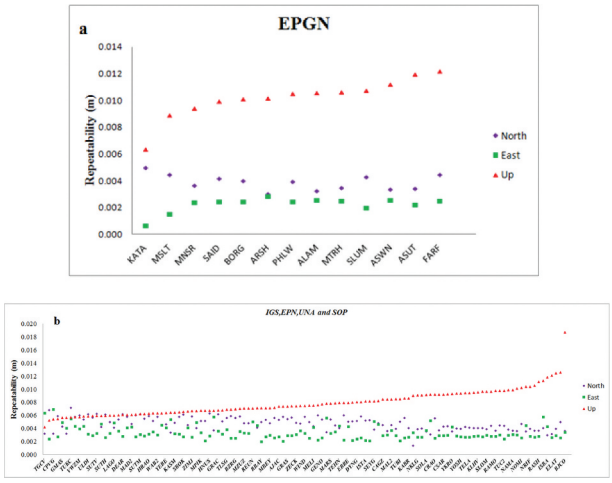

Figure 8. (a) Repeatability of EPGN stations and (b) repeatability of IGS, EPN, UNA and SOP stations.

4.2. Time series analysis and realistic CATS error estimation

A strategy for coordinate time series analysis had been applied to define an accurate velocity with realistic uncertainties. In order to gain most accurate parameter estimates of station motion, different stochastic models were used here to compute more realistic error bounds for all parameters. The approach gave a pre-processing of the coordinate time series in which outliers and discontinuities (mean value, periodic terms with frequencies of annual and semi-annual) were identified. The time series process in the absence of time correlation is white noise (WN). In case of time correlation, power-law noise can be applied. This is a one-dimensional stochastic process whose behaviour in the time domain has the form (Agnew 1992).

$$Q_y(f) = Q_0(f/f_0)^i \quad (1)$$

Where f is the spatial or temporal frequency, Q_0 and f_0 being normalising constants, and i being the spectral index. For several phenomena the index i might range from −3 to −1 with the integer cases (i = −1) for flicker noise, (i = −2) for random noise and (i = 0) for white noise (Mandelbrot and Van Ness 1968).

In the analysis of coordinate time series, the model of station movement was used where the position of a point y has been assumed by (Teferle et al. 2008)

$$y(u) = y_0 + w0(u - u0)\sum_{j=1}^{M}\left(h_j u, \vec{y}\right) + \varepsilon(u)) \quad (2)$$

Where u is the time, the origin time (u_0), y_0 the initial coordinate at time u = u0, $w0$ is a constant velocity of point, h_j are geophysical processes which effect the point coordinates and ε (u) is the error term.

(Langbein and Johnson 1997); (Zhang et al. 1997); (Mao et al. 1999); (Williams 2003a) and (Williams et al. 2004) showed that the stochastic analysis of the coordinate time series was done by Maximum likelihood estimation (MLE). The best fitting model for noise is calculated by maximising the probability function of log-likelihood:

$$\ln\left[\mathrm{lik}(\hat{r}, O)\right] = -1/2\left[\ln(\det O) + \hat{r}^T O^{-1}\hat{r} + e\ln(2\pi)\right] \quad (3)$$

With respect to $\hat{r}$ (the post fit residual vector), containing (e) elements and using covariance matrix (O) for observations,

$$O = c^2 I + d^2_i J_i \quad (4)$$

Where, the amplitude scale factor of white noise and power law noise are c and d_i respectively. I, is the identity matrix and power law noise covariance matrix is J_i and was calculated by means of fractional differencing (Hosking 1981) and (Williams 2003a).

(Williams 2008) estimated linear parameters using Create and Analyse Time Series (CATS) software based on the theory of MLE which include velocity, offsets (due to antenna changes or Earthquakes) and annual and semi-annual variations and nonlinear parameters that allow estimation the amplitude of several noises. In this study two stochastic models were used to estimate the linear and non-linear components. These models are white noise which used to estimate **c** (the amplitude scale factor of white noise) and white plus power law noise in order to estimate **a, d_i, i**, the amplitude scale factor of white and power law noise and spectral index respectively.

The estimated parameters of stochastic model, (i) is the spectral index, (c) amplitude of white noise and (d_i) amplitude of power-law noise plotted for every station using the second model as shown in Figure 9. Figures 10–13 illustrate the CATS analysis for PHLW and SLUM stations from EPGN, and WIND and KLHV from the permanent IGS stations. Table 2 shows a comparison between velocities and their uncertainties obtained from Bernese scaled error and the two stochastic models.

5. GPS results

The Bernese combined solution of about 136 stations for the period 2013–2014 was processed by CATS using two stochastic models as mentioned above. Here the CATS analysis of the second model (white noise + power law noise) was selected as it estimates all parameters in equation (4).

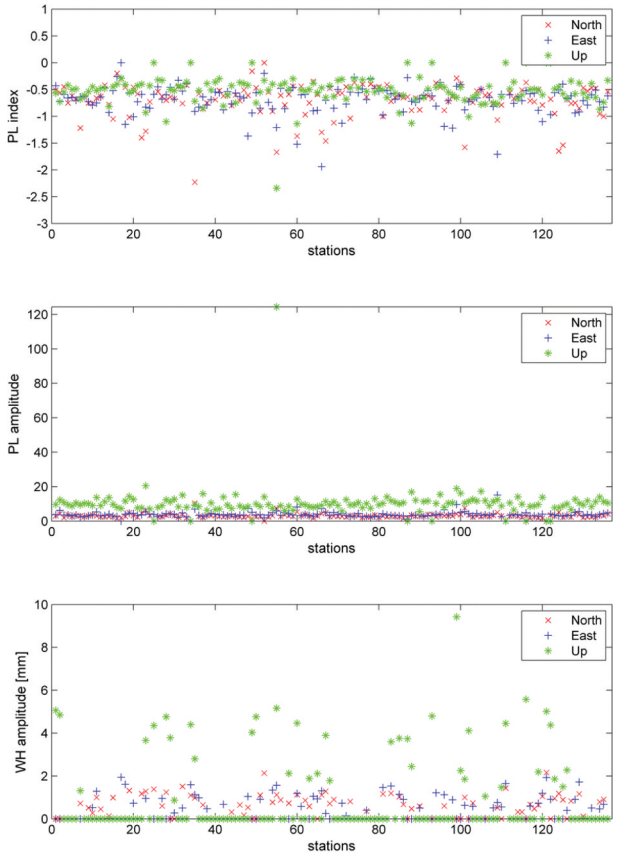

Figure 9. The estimated parameters (a, $\mathbf{d_i}$, **i**) of the white noise plus power-law noise stochastic model.

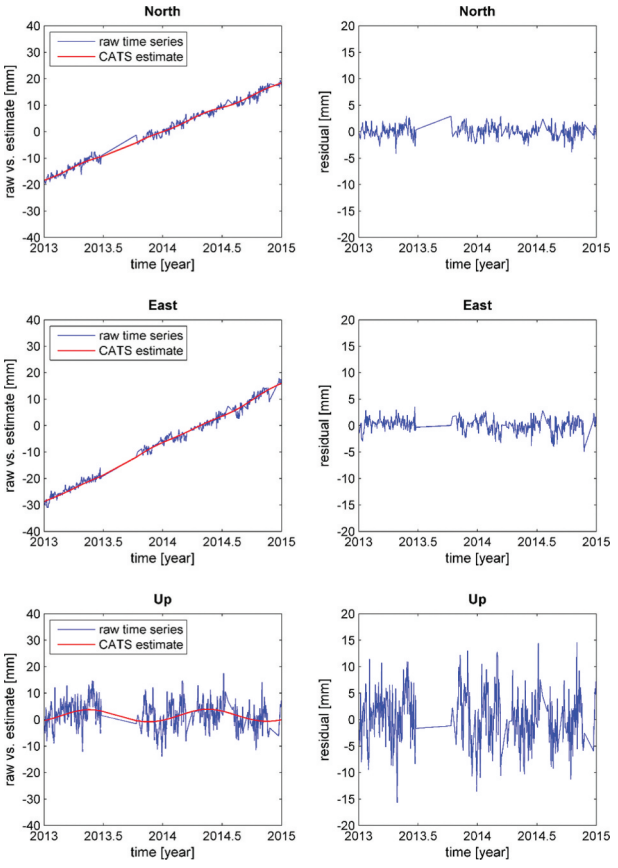

Figure 10. Bernese raw time series (blue line) and the estimated CATS time series (red line) for station PHLW in the left side and residual in the right side in each component using white noise plus power-law noise model.

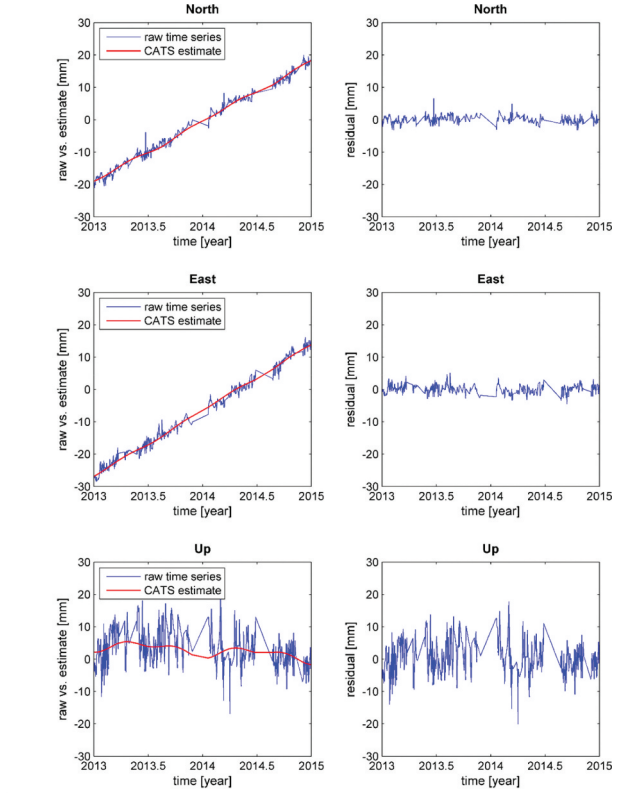

Figure 11. Bernese raw time series (blue line) and the estimated CATS time series (red line) for station SLUM in the left side and residual in the right side in each component using white noise plus power-law noise model.

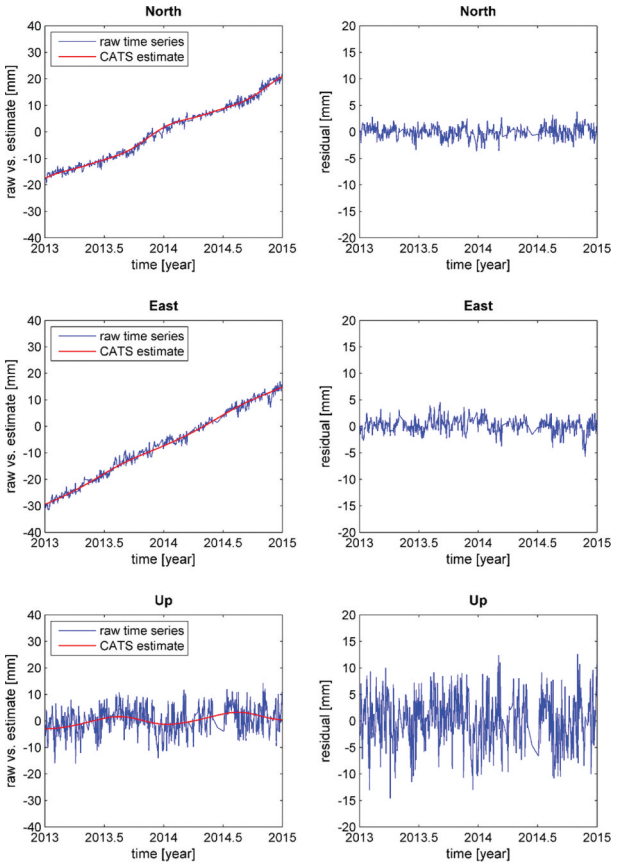

Figure 12. Bernese raw time series (blue line) and the estimated CATS time series (red line) for station KLHV in the left side and residual in the right side in each component using white noise plus power law noise model.

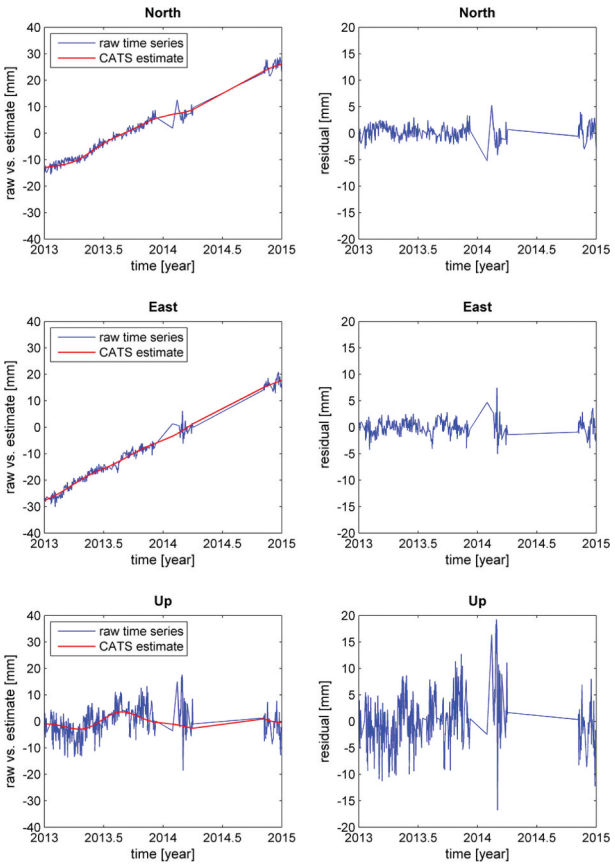

Figure 13. Bernese raw time series (blue line) and the estimated CATS time series (red line) for station WIND in the left side and residual in the right side in each component using white noise plus power law noise model.

Table 2. Velocities and their standard deviations from Bernese scaled error, white noise and white noise plus power law noise stochastic models in mm/yr.

Station	Component	Bernese scaled error	CATS white noise	CATS white noise + power law noise
PHLW	East	27.70 ± 6.99	22.02 ± 0.13	22.38 ± 0.46
	North	22.95 ± 4.74	18.33 ± 0.12	18.41 ± 0.36
	Up	−1.43 ± 9.81	−0.75 ± 0.51	0.16 ± 1.62
SLUM	East	25.61 ± 7.26	20.12 ± 0.14	20.38 ± 0.4
	North	23.38 ± 4.90	18.59 ± 0.12	18.67 ± 0.33
	Up	−2.35 ± 9.80	−2.76 ± 0.53	−1.94 ± 1.59
WIND	East	24.19 ± 5.92	22.93 ± 0.17	22.70 ± 0.47
	North	18.55 ± 6.96	19.48 ± 0.16	19.58 ± 0.45
	Up	2.36 ± 9.30	0.66 ± 0.59	0.18 ± 1.40
KLHV	East	28.06 ± 6.90	21.87 ± 0.11	22.15 ± 0.46
	North	23.11 ± 5.18	19.30 ± 0.09	19.26 ± 0.27
	Up	2.04 ± 7.57	1.18 ± 0.38	1.63 ± 1.06

5.1. Horizontal velocity field

Figures (14) and (15) and Table 3 illustrates that the absolute horizontal velocity in ITRF2008 for the processed stations are significant with 95% of the confidence level. Almost all the Egyptian stations move with magnitude of 28–30 ± 0.7 mm/yr in the northeast direction.

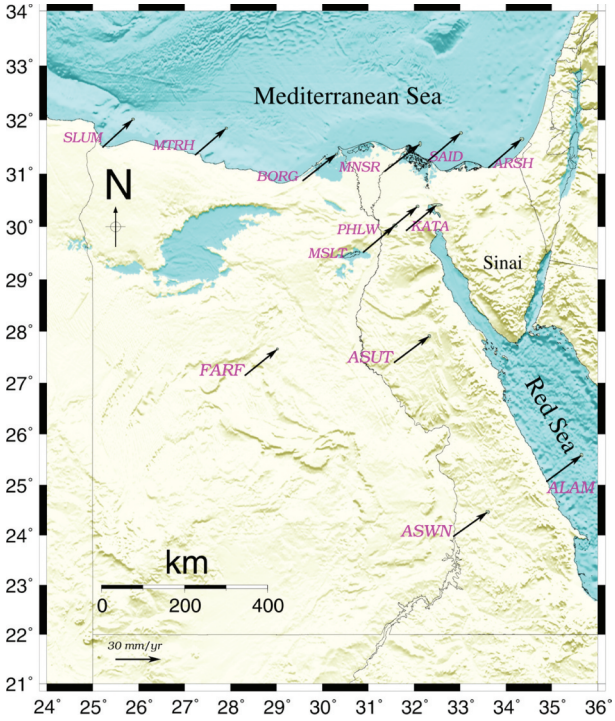

Figure 14. Estimated ITRF2008 horizontal velocities for the processed stations with 95% confidence level.

5.2. Relative or residual velocity field in Nubia fixed frame

For geological interpretation, the absolute velocity field is not valuable. Thus, this velocity is transformed into relative velocity that can be geologically interpreted. In order to estimate the relative motion, we calculated the plate movement for each GPS sites based on absolute ITRF 2008 Euler vectors (longitude (**λ**), latitude (φ) and angular velocity (ω)) that were computed by (Saleh and Becker 2015). It's clear that of the Egyptian sites are showing negligible velocity with respect to Nubia as presented in Figure 16. Residual velocities at stations ARSH, ALAM, ASUT, ASWN, BORG, FARF, MNSR and PHLW are less than 1 mm/yr. On the other hand, few stations show local movement ranges from 1 to 2 mm/yr such as MTRH, SLUM and SAID. Whereas KATA and MSLT show high rates of residual velocities of 2–4 mm/yr which could be related to the short observation period used from these two sites as shown in Figure 6.

5.3. Relative velocity field in Eurasia fixed frame

Relative velocities, with respect to Eurasia, for EPGN stations were estimated using Euler vector parameters which computed by (Saleh and Becker 2015) as shown in Figure 17 and Table 4. Almost all the Egyptian sites are moving towards north to northwest direction with an average rate of 6.7 ± 0.6 mm/yr. As an exception,

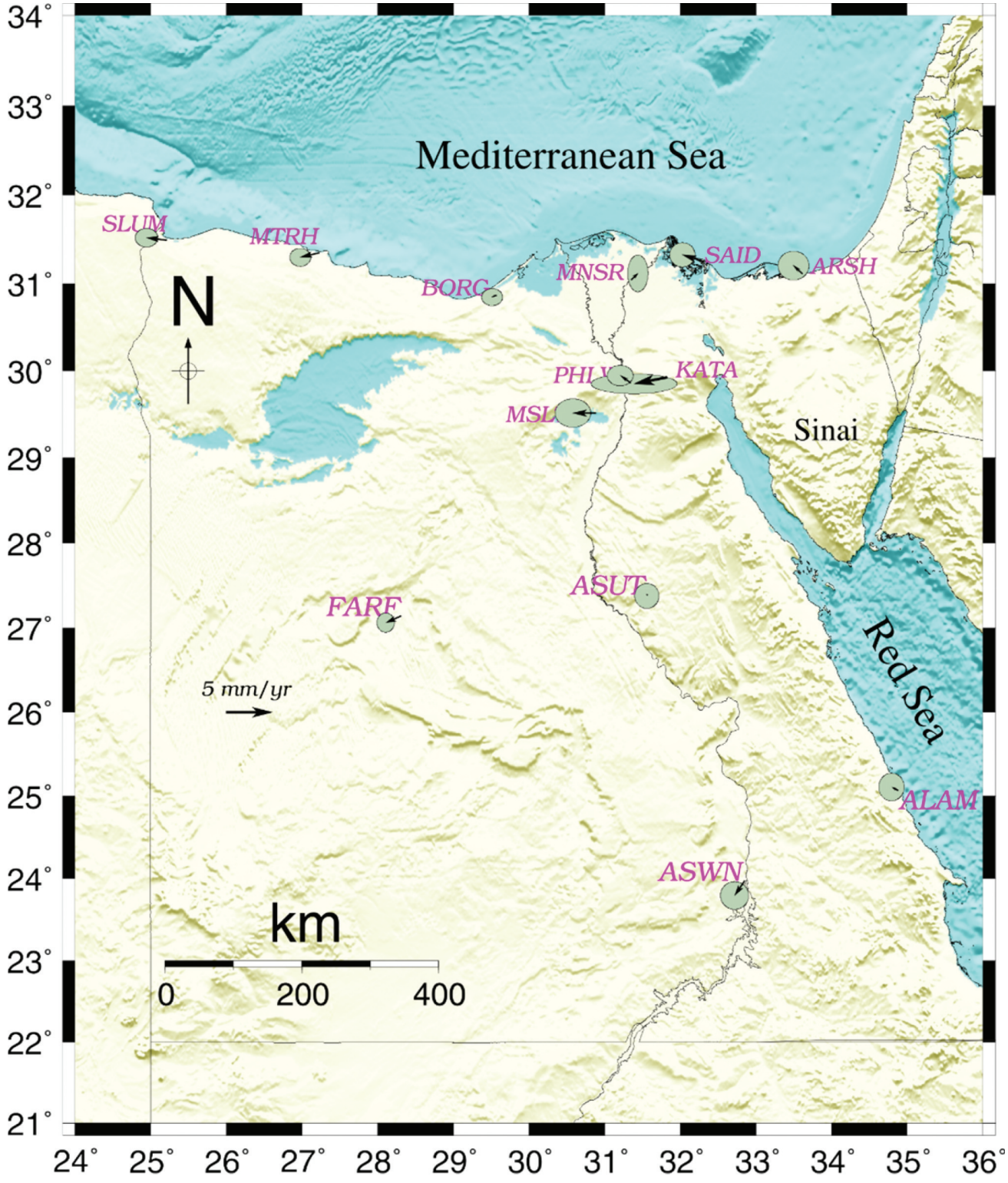

Figure 15. ITRF2008 horizontal velocities of EPGN stations with 95% of the confidence level.

ARSH, located in the Sinai Peninsula, is moving towards northwest direction at a higher rate of 8.7 ± 0.7 mm/yr. By comparing these results with (Saleh and Becker 2014) and (Saleh and Becker 2015), we find that the average difference in most GPS sites is much higher than them with about 1.7 mm/yr and about 0.2 mm/yr, respectively, as presented in Figure 17 and Table 5.

6. Comparison between this result and the previous studies

By comparing the obtained results with (Saleh and Becker 2015), as shown in Table 6, we found that the differences are negligible for most of sites within 1 mm level except for few EPGN stations, the difference reaches to 2–3 mm for KATA and MSLT stations. The reason for this difference may be due to the

Table 3. CATS velocities (ITRF2008) and uncertainties of the (EPGN) stations and the selected stations (IGS, UNA, SOP and EPN) using stochastic model white noise plus power law noise.

Station	long	lat	*Ve* (mm/yr)	*σe* (mm)	*Vn* (mm/yr)	*σn* (mm)
ABPO	47.23	−19.02	19.6	0.45	15.86	0.39
ADIS	38.77	9.04	27.4	0.82	18.55	0.50
AJAC	8.76	41.93	21.29	0.41	14.88	0.21
ALAM	34.88	25.07	23.49	0.45	17.57	0.49
ALON	34.61	31.71	21.54	0.36	19.04	0.30
ALWJ	36.378	26.46	27.93	0.46	24.03	0.41
ANKR	32.76	39.89	1.72	0.31	8.44	0.66
ARSH	33.62	31.11	22.26	0.55	19.17	0.51
ASUT	31.56	27.39	23.47	0.43	17.63	0.44
ASWN	32.85	23.97	22.99	0.50	16.32	0.49
BJCO	2.45	6.39	24.77	0.79	18.77	0.42
BORG	29.57	30.86	22.51	0.37	17.85	0.30
BSHM	35.02	32.78	20.88	0.35	19.48	0.27
BUCU	26.13	44.46	21.15	0.62	11.03	0.37
BZRG	11.34	46.49	20.07	0.32	14.16	0.48
CAGL	8.97	39.14	7.10	8.55	11.40	5.07
CAGZ	8.97	39.14	12.68	0.001	13.28	6.60
CGGN	9.12	10.12	22.90	1.16	19.25	0.45
CPVG	−22.94	16.73	21.72	1.04	14.37	1.41
CRAO	33.99	44.41	24.11	0.76	11.78	0.37
CSAR	34.89	32.49	21.23	0.5	19.42	0.31
CTPM	33.26	−9.70	15.26	1.01	16.61	2.14
DAKR	−17.44	14.72	22.41	0.78	14.39	1.44
DEAR	23.99	−30.67	18.42	0.58	21.66	0.43
DJIG	42.85	11.53	35.41	8.64	28.33	0.001
DRAG	35.39	31.59	21.67	0.28	19.80	0.27
DSEA	35.37	31.04	22.84	0.41	21.83	0.32
DYNG	23.93	38.08	6.93	0.53	−12.57	0.47
EBRE	0.49	40.82	21.10	0.44	15.15	0.53
ELAT	34.92	29.51	23.35	0.5	20.68	0.39
FARF	28.31	27.15	21.72	0.31	17.54	0.34
FUNC	−16.91	32.65	15.77	0.54	16.58	0.53
GENO	8.92	44.42	20.92	0.24	14.85	0.20
GRAC	6.92	43.75	15.27	1.08	5.66	10.57
GRAS	6.92	43.76	21.75	0.48	14.51	0.32
GRAZ	15.49	47.07	21.66	0.32	13.86	0.32
HARB	27.71	−25.89	19.55	0.48	21.48	0.43
HNUS	19.22	−34.43	18.78	0.55	21.66	0.40
HRAO	27.69	−25.89	20.41	0.46	21.32	0.40
Station	long	lat	*Ve* (mm/yr)	*σe* (mm)	*Vn* (mm/yr)	*σn* (mm)
HRMN	35.79	33.31	19.25	0.42	22.42	0.31
IENG	7.64	45.02	21.12	0.34	14.42	0.32
ISBA	44.44	33.34	24.36	0.84	27.71	0.68
ISTA	29.02	41.10	22.21	0.31	11.41	0.32
JSLM	35.20	31.77	22.07	0.42	19.19	0.33
KABR	35.15	33.02	21.18	0.41	19.24	0.23
KASM	31.23	−10.17	22.88	2.23	19.44	0.38
KATA	31.83	29.93	20.47	1.52	17.15	0.35
KATZ	35.69	32.99	21.16	0.40	22.65	0.27
KFNY	35.10	−9.55	24.96	0.59	18.94	0.53
KLHV	34.87	31.38	22.15	0.46	19.26	0.27
LAGO	−8.67	37.09	18.48	0.74	15.75	0.48
LAMP	12.61	35.50	18.29	1.28	20.12	3.13
LIVA	34.11	−10.61	22.08	0.91	17.58	0.80
LROC	−1.22	46.16	19.36	0.76	14.65	0.52
MAD2	−4.25	40.43	18.95	0.48	14.93	0.36
MADR	−4.25	40.43	15.65	1.59	12.48	1.27
MAL2	40.19	−2.99	22.95	2.70	19.27	1.42
MARS	5.35	43.28	21.29	0.37	15.10	0.31
MAS1	−15.63	27.76	18.01	0.47	16.94	0.65
MAT1	16.71	40.65	22.55	0.35	16.61	0.39
MATE	16.70	40.65	22.76	0.46	17.88	0.18
MAUA	23.53	−19.90	22.16	0.61	21.09	0.35
MBAR	30.74	−0.60	25.40	4.69	17.26	1.06
MBBC	34.80	−11.27	22.47	0.64	16.52	1.48
MBEY	33.46	−8.91	25.23	0.37	19.01	0.34
MEDI	11.65	44.52	23.83	0.73	17.37	0.56
MELI	−2.95	35.28	18.38	0.42	17.41	0.33
MFKG	25.54	−25.81	20.16	0.89	21.93	0.31
MIKL	31.97	46.97	21.81	0.46	11.94	0.24
MNSR	31.35	31.04	23.74	0.36	18.33	0.65
MOIU	35.29	0.29	25.74	0.40	17.67	0.43
MPIK	31.45	−11.82	24.11	0.62	20.29	0.40
MSLT	30.89	29.514	21.22	0.63	17.84	0.50
MTRH	27.23	31.35	20.82	0.37	17.88	0.32
MZUZ	34.01	−11.43	24.28	0.31	18.70	0.34

(*Continued*)

Table 3. (Continued).

NAMA	42.05	19.21	33.80	0.52	26.98	0.59
NICO	33.39	35.14	17.73	0.29	15.52	0.22
NKLG	9.67	0.354	24.82	0.73	20.05	0.54
NOMI	25.43	36.42	20.45	0.48	−17.69	0.31
NOT1	14.99	36.88	19.19	0.42	21.13	0.41
Station	long	lat	*Ve* (mm/yr)	*σe* (mm)	*Vn* (mm/yr)	*σn* (mm)
NRIF	35.04	30.04	23.76	0.39	19.96	0.33
NURK	30.09	−1.95	28.07	0.38	18.70	0.32
ORID	20.79	41.13	23.09	0.47	10.78	0.21
PADO	11.89	45.41	20.15	0.42	14.67	0.52
PHLW	31.34	29.86	22.38	0.46	18.41	0.36
RABT	−6.85	33.99	17.85	0.45	16.45	0.49
RAMO	34.76	30.59	22.57	0.32	18.98	0.32
RASH	34.79	28.29	25.83	0.35	22.48	0.46
RBAY	32.08	−28.79	10.29	3.65	19.12	4.25
RCMN	36.89	−1.22	27.59	0.68	18.23	0.30
REUN	55.57	−21.21	15.76	0.37	14.13	0.39
ROAP	−6.21	36.46	16.52	1.37	15.69	0.45
SAID	32.31	31.25	21.43	0.45	18.25	0.43
SBOK	17.88	−29.66	19.83	0.99	21.66	0.35
SEY1	55.48	−4.67	24.27	1.29	11.39	0.53
SEYG	55.53	−4.67	24.25	0.53	12.23	0.39
SFER	−6.21	36.46	21.96	0.82	21.43	2.73
SLOM	34.28	31.23	20.51	0.56	19.36	0.44
SLUM	25.21	31.49	20.38	0.40	18.67	0.33
SNGC	35.67	−10.69	22.89	0.57	19.12	0.36
SOFI	23.39	42.56	22.75	0.44	11.06	0.35
SOLA	46.40	24.91	30.96	0.49	28.90	0.40
SPIR	35.18	30.61	22.13	0.50	19.76	0.39
SUTH	20.81	−32.38	20.88	0.59	21.59	0.46
SUTM	20.81	−32.38	20.19	6.78	21.44	0.91
SUTV	20.81	−32.38	20.40	0.52	21.56	0.65
TANZ	39.21	−6.77	16.18	0.001	22.50	0.001
TAYS	34.87	28.55	25.71	0.39	22.48	0.33
TDOU	30.38	−23.08	19.36	0.55	21.25	0.47
TEHN	51.33	35.69	24.87	0.44	20.33	0.36
TELA	34.78	32.07	21.96	0.42	19.14	0.23
TLSE	1.48	43.56	20.58	0.36	14.53	0.24
TLSG	1.49	43.55	26.84	5.75	14.08	4.89
TUBI	29.45	40.79	18.00	0.44	11.31	0.22
ULDI	31.42	−28.29	17.72	0.66	20.72	0.45
VILL	−3.95	40.44	19.83	0.42	14.10	0.50
VWZM	33.57	−11.18	20.82	0.74	14.63	3.08
WAB2	7.46	46.92	20.45	0.30	14.33	0.77
WIND	17.09	−22.58	22.70	0.47	19.59	0.46
YEBE	−3.09	40.53	20.20	0.39	14.02	0.32
Station	long	lat	*Ve* (mm/yr)	*σe* (mm)	*Vn* (mm/yr)	*σn* (mm)
YIBL	56.11	22.19	32.96	0.80	33.36	0.62
YKRO	−5.24	6.87	24.92	1.12	17.73	0.70
YOSH	35.21	32.10	21.77	0.41	19.79	0.23
YRCM	34.93	30.99	23.00	0.53	18.84	0.27
ZAMB	28.31	−15.43	21.90	0.42	19.62	0.28
ZECK	41.57	43.79	24.19	0.28	11.58	0.25
ZIM2	7.47	46.88	17.85	0.48	11.79	0.57
ZIMJ	7.47	46.88	20.43	0.81	14.18	0.67
ZOMB	35.33	−15.38	21.32	0.57	18.53	0.48

short period of observations used in this work as shown in Figure 6.

7. Conclusion

n this work, we processed 13 permanent GPS stations from EPGN, which cover the time interval from the first of January, 2013 to the end of December, 2014, with 123 permanent stations from various sources (EPN, IGS, UNA and SOP) linking to three different tectonic plates (African, Arabian and Eurasian). 31 stations out of these 123 are occurred in ITRF2008 and were used for datum definition. From Bernese combined solution, the proportion between formal standard deviation and the repeatability were used in order to estimate the covariance matrix scale that ended to compute the scaled error. Due to the unrealistic uncertainties of Bernese result and to handle the absence of time correlation in GNSS result, modern approach was applied in order to evaluate the achieved solution by taking into account the time correlation in GNSS time series. For the time series analysis, CATS was applied with two stochastic models. These models are white noise and white plus power law noise. We considered the second model for assessing our results

Figure 16. Relative velocities of EPGN stations in Nubia fixed frame with 95% of the confidence level.

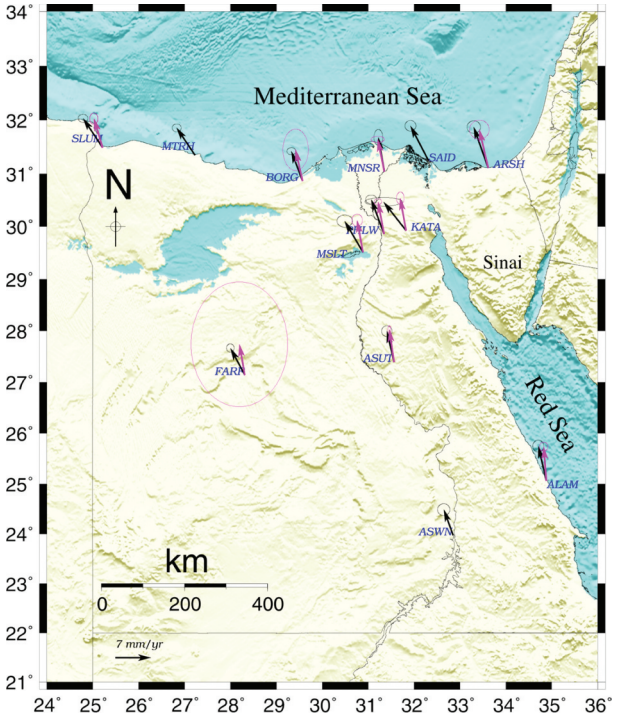

Figure 17. Velocities in Eurasia fixed frame with 95% confidence, black vectors estimated from current study and violet vectors after (Saleh and Becker 2015).

Table 4. GPS horizontal velocities in Eurasia-fixed reference frame for EPGN sites.

Station	Long	Lat	*Ve* (mm/yr)	*σe* (mm)	*Vn* (mm/yr)	*σn* (mm)
ALAM	34.88	25.07	−1.58	0.45	6.88	0.49
ARSH	33.62	31.11	−2.90	0.55	8.18	0.51
ASUT	31.56	27.39	−1.42	0.43	6.16	0.44
ASWN	32.85	23.97	−1.86	0.50	5.15	0.49
BORG	29.57	30.86	−2.24	0.37	5.94	0.30
FARF	28.31	27.15	−2.86	0.31	5.35	0.34
KATA	31.83	29.93	−4.50	1.52	5.74	0.35
MNSR	31.35	31.04	−1.19	0.36	6.82	0.65
MSLT	30.89	29.51	−3.65	0.63	6.22	0.50
MTRH	27.23	31.35	−3.67	0.37	5.46	0.32
PHLW	31.34	29.86	−2.54	0.46	6.89	0.36
SAID	32.31	31.25	−3.60	0.45	6.96	0.43
SLUM	25.21	31.49	−3.87	0.40	5.83	0.33

Table 5. Comparison between velocities and uncertainties in mm/yr estimated from current study and (Saleh and Becker 2015) for EPGN stations in Eurasia fixed frame.

	Eurasia-fixed reference frame				Saleh and Becker., 2015				Difference	
Station	*ve*	*vn*	*σe*	*σn*	*ve*	*vn*	*σe*	*σn*	*ve*	*vn*
ALAM	−1.58	6.87	0.45	0.49	−0.51	6.77	0.34	0.37	−1.07	−0.10
ARSH	−2.90	8.17	0.55	0.51	−1.78	7.67	0.80	0.78	−1.12	−0.50
ASUT	−1.42	6.16	0.43	0.44	−0.92	6.45	0.12	0.33	−0.50	0.29
BORG	−2.23	5.93	0.37	0.30	−1.40	6.24	1.04	1.69	−0.83	−0.31
FARF	−2.85	5.35	0.31	0.34	−1.06	6.10	3.94	5.10	−1.79	−0.75
KATA	−4.50	5.74	1.52	0.35	−1.17	6.47	0.31	0.50	−3.33	−0.73
MNSR	−1.19	6.81	0.36	0.65	−1.32	6.42	0.54	0.26	0.13	0.39
MSLT	−3.65	6.22	0.63	0.50	−1.18	6.38	0.43	0.50	−2.47	−0.16
PHLW	−2.54	6.89	0.46	0.36	−1.19	6.42	0.30	0.25	−1.35	0.47
SLUM	−3.87	5.83	0.40	0.33	−1.71	5.76	0.34	0.46	−2.16	0.07

Table 6. Comparison between velocities and uncertainties in mm/yr from CATS (WH plus power law noise) and (Saleh and Becker 2015) results for EPGN stations.

	Saleh and Becker, 2015				WH + PL N				Difference	
Station	*ve*	*vn*	*σe*	*σn*	*ve*	*vn*	*σe*	*σn*	*ve*	*vn*
ALAM	25.80	18.38	0.34	0.37	23.49	17.57	0.45	0.49	2.31	0.81
ARSH	25.20	19.60	0.80	0.78	22.26	19.17	0.55	0.51	2.94	0.43
ASUT	22.97	18.06	0.12	0.33	23.47	17.63	0.43	0.44	−0.50	0.43
BORG	21.73	16.66	1.04	1.69	22.51	17.85	0.37	0.30	−0.78	−1.19
FARF	23.40	21.50	3.94	5.10	21.72	17.54	0.31	0.34	1.68	3.96
KATA	24.57	18.53	0.31	0.50	20.47	17.15	1.52	0.35	4.10	1.38
MNSR	25.82	20.14	0.54	0.26	23.74	18.33	0.36	0.65	2.08	1.81
MSLT	23.46	16.95	0.43	0.50	21.22	17.84	0.63	0.50	2.24	−0.89
PHLW	21.61	17.99	0.30	0.25	22.38	18.41	0.46	0.36	−0.77	−0.42
SLUM	21.73	18.79	0.34	0.46	20.38	18.67	0.40	0.33	1.35	0.12

as it offers the estimation of all stochastic parameters (spectral index, amplitude of white noise and power law noise (i, c^2, d^2_i)). Therefore, the velocities and uncertainties of this model were used. Almost all the Egyptian stations move with magnitude 28–30 ± 0.7 mm/yr. in the NE direction in ITRF2008. With respect to Nubia, most of the Egyptian sites show negligible motion. On the other hand, an average velocity rate of 6.7 ± 0.6 mm/yr is estimated with respect to Eurasia. The comparison between this result and (Saleh and Becker 2015) showed little differences in the estimated velocities except for few stations such as KATA and MSLT due to the lack of observations during the time of study. Therefore, with using only two years of continuous GPS data, we were able to estimate comparable velocity rates to the previously published rates from longer period of data.

Acknowledgements

The authors are grateful to the staff of Physical and Satellite Geodesy Institute (PSGD), TU-Darmstadt, Germany. Also, the authors are thankful to scientific and Technology Development fund (STDF) in Egypt for supporting this work through the project no (6933). We greatly appreciate the staff members of the Geodynamics department, NRIAG, especially for their help in the data gathering. Most of the maps in this paper were prepared using the Generic Mapping Tools (GMT) software [42].

Disclosure statement

No potential conflict of interest was reported by the authors.

ORCID

Nadia AbouAly http://orcid.org/0000-0002-8922-2261
Matthias Becker http://orcid.org/0000-0002-4816-7470
Mohamed Saleh http://orcid.org/0000-0003-3482-7703

References

Abd El-AaL K. 2010. Ground motion prediction from nearest seismogenic zones in and around greater Cairo Area, Egypt. Nat Hazards Earth Syst Sci. 10:1495–1511. doi:10.5194/nhess-10-1495-2010

Abd El-Motaal E, Kusky M. 2003. Tectonic evolution of the intraplate S-shaped Syrian Arc fold-thrust belt of the Middle East region in the context of plate tectonics. 3rd International Conference on the Geology of Africa, Assuit, Egypt, Vol. (2), p. 139–157.

Abou Elenean K. 1997. Seismotectonics of Egypt in relation to the Mediterranean and red sea tectonics. Ph.D. Thesis, Faculty of Science, Ain Shams University, Egypt.

Abou Elenean K. 2007. Focal mechanisms of small and moderate size earthquakes recorded by the Egyptian National Seismic Network (ENSN), Egypt, NRIAG. J Geophys. 6(1):119–153.

Abudeif A, Attia M. 2014. Seismic hazards assessment for engineering characterization of the northern part of Egypt. J Geophys Eng. (Article reference: JGE-100407).

Agnew D. 1992. The time-domain behavior of power-law noises. Geophys Res Lett. 19:333–336. doi:10.1029/91GL02832.

Altamimi Z, Collilieux X, Metivier L. 2011. ITRF2008: an improved solution of the international terrestrial reference frame. J Geod. 85:457–473. doi:10.1007/s00190-011-0444-4

Badawy A. 2005. Seismicity of Egypt. Seismol Res Lett. 76:149–160. doi:10.1785/gssrl.76.2.149.

Badawy A, El-Hady S, Abdel Fattah A. 2008. Microearthquakes and neotectonics of Abu-Dabbab, Eastern Desert of Egypt. Seismol Res Lett. 79:55–67. doi:10.1785/gssrl.79.1.55

Badawy A, Gad M, Khaled O, Walid F. 2015. The northern Egyptian continental margin. J Afr Earth Sci. 101:177–185. doi:10.1016/j.jafrearsci.2014.09.009

Dach R, Hugentobler U, Fridez P, Meindl M. 2007. Bernese GPS software version 5.0. manual. Astronomical Institute, University of Berne.

Gergawi A, El Khashab H. 1968. Seismicity of the U.A.R. Helwan observatory bull. 76.

Harms C, Wray L. 1990. Nile delta. In: Said R, editor. The geology of Egypt. Roterdam: Balkema; p. 329–343.

Hosking M. 1981. Fractional differencing. Biometrika. 68 (1):165–176. doi:10.1093/biomet/68.1.165.

Hussein M, Marzouk I, Moustafa A, Hurukawa N. 2006. Preliminary seismicity and focal mechanisms in the southern Gulf of Suez: August 1994 through December 1997. J Afr Earth Sci. 45:48–60. doi:10.1016/j.jafrearsci.2006.01.006

Kebeasy R. 1990. Seismicity. In: Said R, editor. The geology of Egypt. Rotterdam: A. A. Balkema; p. 51–59.

Langbein J, Johnson O. 1997. Correlated errors in geodetic time series: implications for time-dependent deformation. J Geophys Res. 102:591–603. doi:10.1029/96JB02945.

Mandelbrot B, Van Ness J. 1968. Fractional Brownian motions, fractional noises, and applications. SIAM Rev. 10:422–439. doi:10.1137/1010093.

Mao A, Harrison C, Dixon H. 1999. Noise in GPS coordinate time series. J Geophys Res. 104:2797–2818. doi:10.1029/1998JB900033.

McClusky S, Balassanian S, Barka A. 2000. Global positioning system constraints on plate kinematics and dynamics in the eastern Mediterranean and Caucasus. J Geophys Res. 105(B3):5695–5720. doi:10.1029/1999JB900351.

McClusky S, Reilinger R, Mahmoud S, Ben Sari D, Tealeb A. 2003. GPS constraints on Africa (Nubia) and Arabia plate motions. J Geophys Int. 155:126–138. doi:10.1046/j.1365-246X.2003.02023.x

Meshref M. 1999. Cretaceous tectonics and its impact on oil exploration in northern Egypt. In: Geological society of Egypt. Vol. 2. Special Publication; p. 199–244.

Mohamed EK, Hassoup A, Abou EK, Othman A, Hamed D. 2015. Earthquakes focal mechanism and stress field pattern in the northeastern part of Egypt. NRIAG J Astron Geophys. 4:205–221. doi:10.1016/j.nrjag.2015.09.001

Mosconi A, Rebora A, Venturino G, Bocc P. (1996): Egypt -Nile delta and north Sinai, Cenozoic tec- tonic evolutionary model, a proposal. European Association of Geoscientists & Engineers, Conference Proceedings, 58th EAGE Conference and Exhibition, ISBN: 978-90-73781-07-8. doi:10.3997/2214-4609.201409027.

Neev D. 1977. The Pelusium line, a major transcontinental shear. Tectonophysics. 38:T1–T8. doi:10.1016/0040-1951(77)90207-4.

Orwig E. 1982. Tectonic framework of northern Egypt and the eastern Mediterranean region: The Egyptian General Petroleum Corporation; p. 567–606. Ed. du Museum National d'Histoire Naturelle, Paris.

Plag H. 1998. Scientific objectives of current and future WEGENER activities. Tectonophysics. 294(3–4):177–223. doi:10.1016/S0040-1951(98)00100-0.

Reilinger RE, McClusky S, Vernant P, Lawrence S, Ergintav S, Cakmak R, Ozener H, Kadirov F, Guliev I, Stepanyan R, et al. 2006. GPS constraints on continental deformation in the Africa-Arabia- Eurasia continental collision zone and implications for the dynamics of plate interactions. J Geophys Res. 111:B05411. doi:10.1029/2005JB004051

Said R. 1962. The geology of Egypt. Amsterdam: Elsevier Pub. Co.; p. 377.

Said R. 1990. The geology of Egypt. Rotterdam: A. A. Balkema.

Saleh M, Becker M. 2014. A new velocity field from the analysis of the Egyptian permanent GPS network (EPGN). Arab J Geosci. doi:10.1007/s12517-0131132-x

Saleh M, Becker M. 2015. New constraints on the Nubia–Sinai–Dead Sea fault crustal motion. Tectonophysics. 651–652:79–98. doi:10.1016/j.tecto.2015.03.015

Sawires R, Peláez J, Fat-Helbary R, Ibrahim H. 2016. An earthquake catalogue (2200 B.C. to 2013) for seismotectonic and seismic hazard assessment studies in Egypt. In: D'Amico S, editor. Earthquakes and their impact on society. Cham: Springer Natural Hazards. Springer; doi:10.1007/978-3-319-21753-6_4.

Sieberg A. 1932. Erdbebengeographie, Handbuch der Geophysik, Band IV, Abschnitt VI. Germany: Berlin.

Stanley J, Goodfriend A. 1997. Recent subsidence of the northern Suez Canal. Nature. 388:335–336. doi:10.1038/40997.

Teferle N, William S, Kierulf P, Bingley R, Plag P. 2008. A continuous GPS coordinate time series analysis strategy for high-accuracy vertical land movements. Phys Chem Earth. 33:205–216. doi:10.1016/j.pce.2006.11.002

Wessel P, Smith H. 1995. The generic mapping tools (GMT). EOS Trans Am Geophys Union. 76:329. doi:10.1029/95EO00198.

Williams P. 2003a. The effect of coloured noise on the uncertainties of rates estimated from geodetic time series. J Geodesy. 76:483–494.

Williams P. 2008. CATS: GPS coordinate time series analysis software. GPS Solutions. 12:147–153. doi:10.1007/s10291-007-0086-4

Williams P, Bock Y, Fang P, Jamason P, Nikolaidis RM, Prawirodirdjo L, Miller M, Johnson J. 2004. Error analysis of continuous GPS position time series. J Geophys Res. 109:B03412. doi:10.1029/2003JB002741

Zeyen H, Volker F, Wehrle V, Fuchs K, Sobolev S, Altherr R. 1997. Styles of continental rifting crust-mantle detachment and mantle plumes. Tectonophysics. 278(1997):329–352. doi:10.1016/S0040-1951(97)00111-X.

Zhang J, Bock Y, Johnson H, Fang P, Williams S, Genrich J, Wdowinski S, Behr J. 1997. Southern California permanent GPS geodetic array: error analysis of daily position estimates and site velocities. J Geophys Res. 102 (B8):18035–18055. doi:10.1029/97JB01380.

Appendix A

Table 1A: Helmert Transformation

NUM	NAME	FLG	RESIDUALS IN MILLIMETERS		
9	ANKR 20805M002	I W	0.64	17.65	1.01
18	BUCU 11401M001	I W	-3.35	0.57	-2.86
20	CAGL 12725M003	I W	-0.99	-3.07	-0.69
21	CAGZ 12725M004	I W	-0.30	-3.95	-6.18
24	CRAO 12337M002	I W	-3.52	-0.36	1.61
30	DRAG 20710S001	I W	6.84	-3.82	-0.71
40	GMAS 31303S004	I W	-1.04	-5.72	4.15
42	GRAS 10002M006	I W	-0.69	0.98	-4.01
43	GRAZ 11001M002	I W	-2.83	-0.21	-7.63
45	HARB 30302M009	I W	0.06	3.03	1.84
48	HRAO 30302M004	I W	0.82	-1.29	-3.83
56	ISTA 20807M001	I W	-0.82	0.59	-4.72
72	LROC 10023M001	I W	2.20	2.18	1.35
79	MAS1 31303M002	I W	3.81	-2.60	2.21
80	MAT1 12734M009	I W	-0.95	-1.26	-1.55
81	MATE 12734M008	I W	-4.91	1.63	-2.08
86	MEDI 12711M003	I W	-1.90	-1.99	-0.37
100	NICO 14302M001	I W	-5.14	3.80	4.63
101	NKLG 32809M002	I W	0.87	0.11	2.23
114	RABT 35001M002	I W	3.97	-0.77	1.19
115	RAMO 20703S001	I W	7.43	-3.52	2.69
125	SFER 13402M004	I W	-3.04	-0.96	8.49
131	SOFI 11101M002	I W	-1.11	-0.31	0.80
134	SUTH 30314M002	I W	-1.50	3.07	-0.64
136	SUTV 30314M002	I W	-0.68	2.38	0.11
143	TLSE 10003M009	I W	-0.39	0.39	0.31
153	VILL 13406M001	I W	1.89	1.20	0.99
156	WIND 31101M001	I W	1.31	-0.71	0.73
157	YEBE 13420M001	I W	2.81	-0.15	1.35
158	YIBL 25001M001	I W	2.83	-3.51	-2.61
163	ZECK 12351M001	I W	-4.17	-1.27	2.15
	RMS / COMPONENT		3.06	3.98	3.26
	MEAN		-0.06	0.07	-0.00
	MIN		-5.14	-5.72	-7.63
	MAX		7.43	17.65	8.49

NUMBER OF PARAMETERS : 7
NUMBER OF COORDINATES : 93
RMS OF TRANSFORMATION : 3.54 MM